J. Fluid Mech. (1981), *vol.* 108, *pp.* 89–100
Printed in Great Britain

Axisymmetric bubble or drop in a uniform flow

By MICHAEL MIKSIS, JEAN-MARC VANDEN-BROECK
Department of Mathematics Stanford University
AND JOSEPH B. KELLER
Departments of Mathematics and Mechanical Engineering,
Stanford University, Stanford, CA 94305

(Received 12 May 1980 and in revised form 29 September 1980)

The deformation of an axisymmetric bubble or drop in a uniform flow of constant velocity U is computed numerically. The flow is assumed to be inviscid and incompressible. The problem is formulated as a nonlinear integrodifferential system of equations for the bubble surface and for the potential function on the surface. These equations are discretized and the resulting algebraic system is solved by Newton's method. For $U = 0$ the bubble is a sphere. The results show that as U increases the bubble becomes oblate, spreading out in the direction normal to the flow and contracting in the direction of the flow. Then the poles get pushed in and ultimately they touch each other. The results also show that there is a maximum value of the Weber number above which there is no steady axially symmetric bubble. This value is somewhat smaller than the approximate value obtained by Moore (1965) but close to that found by El Sawi (1974). We also compute the added mass, the drag on the bubble, and its terminal velocity in a gravitational field, for large Reynolds numbers.

1. Introduction

We consider the deformation of a gas bubble or liquid drop due to the steady potential flow of an incompressible inviscid fluid around it. We shall write 'bubble' to mean either bubble or drop. Far from the bubble the flow is uniform with a constant velocity U (see figure 1). The bubble is assumed to be axisymmetric around the direction of the flow at infinity. It is characterized by its pressure p_b and its surface tension σ, while the fluid has density ρ and pressure p_∞ at infinity. As we shall see, the shape of the bubble is determined by the dimensionless parameter

$$\gamma = (p_b - p_\infty - \tfrac{1}{2}\rho U^2)/\tfrac{1}{2}\rho U^2. \tag{1.1}$$

The size of the bubble is proportional to the length $2\sigma/\rho U^2$.

For γ large the bubble is asymptotically a sphere. As γ decreases from infinity, the bubble extends in the direction perpendicular to the flow. At first it becomes nearly an oblate spheroid. As γ decreases further, the bubble is pushed inward at its poles. Finally at $\gamma = \gamma_0 \sim -0{\cdot}3$ opposite sides of the bubble touch each other. The bubble shape is then in rough agreement with the slender-body approximation presented by Vanden-Broeck & Keller (1980). For $\gamma < \gamma_0$ the bubble will presumably become a torus.

We shall formulate this flow problem as a boundary-value problem in § 2. Then in § 3 we shall convert it into an integrodifferential equation and in § 4 present a

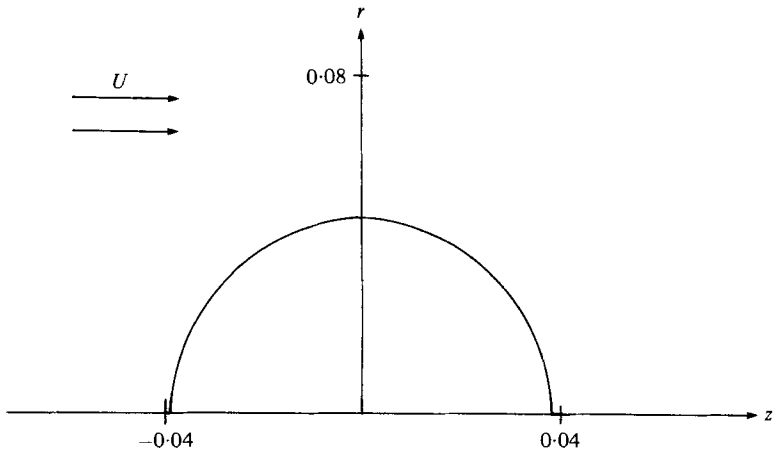

FIGURE 1. Computed profile of an axially symmetric bubble with $\gamma = 50$ in the r, z plane of a cylindrical co-ordinate system. The flow at infinity is along the z axis and has speed U. The unit of length in which r and z are measured is $2\sigma/\rho U^2$, and γ is defined by (1.1).

method for solving this equation numerically. The method involves discretization, which converts the equation into a set of nonlinear algebraic equations. Some of our results are shown in figures 1–7 and they are discussed in § 5 and 6.

For $\gamma > 4$ our numerical results agree with Moore's (1965) results within 10%. He assumed the bubble was a spheroid and determined its axis ratio approximately by satisfying the pressure condition at the pole and equator. His results were confirmed and extended by El Sawi (1974) who used a different approximation based on the virial method. Their results also indicated that there is a maximum value of the Weber number W above which no steady axisymmetric solution exists. Moore and El Sawi have found the value of this maximum to be $W = 3{\cdot}74$ and $W = 3{\cdot}27$ respectively. Our results confirm the existence of such a maximum and yield for its value $W = 3{\cdot}23$.

For each value of $\gamma \geqslant \gamma_0$, we use our computed flow to evaluate the added mass, and also the rate of energy dissipation, assuming that the fluid is viscous. Levich (1949) has shown that this dissipation rate is asymptotically correct for large Reynolds numbers. From it we calculate the drag coefficient of the bubble. By equating the drag to the buoyancy, we find the terminal velocity of the bubble. Upon using this velocity to calculate the Reynolds number, we find results similar to those of Moore (1965) and El Sawi (1974). Since we neglect pressure variations within the bubble or drop, our results apply to a real drop only if its density and viscosity are small compared to those of the surrounding fluid. See Harper & Moore (1968).

2. Formulation as a boundary-value problem

Let us consider the steady potential flow of an inviscid incompressible fluid around a bubble within which the pressure has the constant value p_b (see figure 1). We assume that the bubble is symmetric around the z axis of a cylindrical co-ordinate system and that the flow is along the z axis at infinity. Thus figure 1 represents a cross-section of the bubble. The profile is assumed to be symmetrical around the plane $z = 0$. It is convenient to measure velocities in units of U and lengths in units of $2\sigma/\rho U^2$.

We denote by ϕ the potential function. Without loss of generality we assume

$$\phi = 0 \quad \text{at} \quad r = \rho_M. \tag{2.1}$$

Here ρ_M is the semi-major axis of the bubble. The function ϕ satisfies Laplace's equation in the fluid region. At infinity we require the velocity to be U in the z direction, so that the dimensionless velocity is unity in the z direction. Therefore

$$\phi \sim z \quad \text{at infinity.} \tag{2.2}$$

On the bubble surface the Bernoulli equation and the pressure jump due to surface tension yield

$$p_\infty + \frac{\rho U^2}{2} - \frac{\rho q^2}{2} + \sigma K = p_b, \quad z = \eta(r). \tag{2.3}$$

Here $q = |\nabla\phi|$ is the flow speed, K the mean curvature of the bubble surface counted positive when the bubble is on the concave side of the surface and $z = \eta(r) > 0$ the equation of the profile of the bubble in the first quadrant. In dimensionless variables (2.3) becomes

$$q^2 = K - \gamma, \quad z = \eta(r), \tag{2.4}$$

where γ is defined in (1.1). In addition the normal derivative of ϕ must vanish on the surface of the bubble:

$$\frac{\partial\phi}{\partial n} = 0, \quad z = \eta(r). \tag{2.5}$$

Finally we impose the geometrical conditions

$$\eta(\rho_M) = 0, \quad \dot{\eta}(0) = 0. \tag{2.6), (2.7}$$

This completes the formulation of the problem of determining the function $\eta(r)$ and the harmonic function ϕ. They must satisfy the conditions (2.1), (2.2) and (2.4)–(2.7).

3. Reformulation as an integrodifferential equation

It is convenient to reformulate the boundary-value problem as an integrodifferential equation by considering the function

$$F(r, z) = \phi(r, z) - z. \tag{3.1}$$

The function F satisfies Laplace's equation for $|z| > \eta(r)$ and vanishes at infinity in view of (2.2). We now apply Green's theorem to F and the Green's function g in the domain delimited by the surface of the bubble and a sphere of infinite radius. We use the symmetry about the z axis and write the area element of the bubble surface as $r[1 + \dot{\eta}^2(r)]^{\frac{1}{2}}\, dr\, d\theta$. Then by following Garabedian (1964, p. 348), we obtain

$$\begin{aligned}\alpha F(r_0, z_0) = \int_0^{2\pi}\int_0^{\rho_M} & d\theta\, dr\, r[1 + \dot{\eta}^2(r))]^{\frac{1}{2}} \\ & \times \Big\{F[r, \eta(r)]\frac{\partial g}{\partial n}[r, \theta, \eta(r), r_0, 0, z_0] + F[r, -\eta(r)]\frac{\partial g}{\partial n}[r, \theta, -\eta(r), r_0, 0, z_0] \\ & - g[r, \theta, \eta(r), r_0, 0, z_0]\frac{\partial}{\partial n}F[r, \eta(r)] - g[r, \theta, -\eta(r), r_0, 0, z_0]\frac{\partial}{\partial n}F[r, -\eta(r)]\Big\}.\end{aligned} \tag{3.2}$$

Here
$$\alpha = \begin{cases} 1 & \text{for } |z_0| > \eta(r_0), \\ \frac{1}{2} & \text{for } |z_0| = \eta(r_0). \end{cases}$$

For $|z_0| = \eta(r_0)$, the integral in (3.2) is to be interpreted in the Cauchy-principal value sense. The Green's function g is defined by

$$g(r_1, \theta_1, z_1, r_2, \theta_2, z_2) = -\frac{1}{4\pi}[(r_1 \cos\theta_1 - r_2 \cos\theta_2)^2 + (r_1 \sin\theta_1 - r_2 \sin\theta_2)^2 + (z_1 - z_2)^2]^{-\frac{1}{2}}. \tag{3.3}$$

The differential operator $\partial/\partial n$ in (3.2) denotes the normal derivative along the normal pointing into the bubble.

To simplify (3.2) we use (2.5) and (3.1) to obtain

$$\frac{\partial F}{\partial n} = -\frac{\partial z}{\partial n}. \tag{3.4}$$

We also assume that the bubble is symmetric about the plane $z = 0$, so

$$F[r, -\eta(r)] = -F[r, \eta(r)]. \tag{3.5}$$

Upon substituting (3.1)–(3.5) into (3.2) for $z_0 = \eta(r_0)$ we find after some algebra

$$2\pi[\phi(r_0) - \eta(r_0)] = \int_0^{\rho_M} r\,dr \left\{ \left[(\phi(r) - \eta(r)) \left(-\dot{\eta}(r) \frac{\partial g^-}{\partial r} + \frac{\partial}{\partial \eta(r)} g^- \right) + g^- \right] \right.$$
$$\left. + (\eta(r) - \phi(r)) \left[-\dot{\eta}(r) \frac{\partial g^+}{\partial r} + \frac{\partial}{\partial \eta(r)} g^+ \right] - g^+ \right\}. \tag{3.6}$$

Here
$$g^{\pm} = \int_0^{2\pi} d\theta\, [r_0^2 + r^2 - 2rr_0 \cos\theta + \{\eta(r_0) \pm \eta(r)\}^2]^{-\frac{1}{2}}. \tag{3.7}$$

The integrals in (3.7) can be rewritten in terms of elliptic integrals of the first kind (Miksis 1981).

Next we rewrite (2.4) in the form

$$\left(\frac{\partial \phi}{\partial s}\right)^2 + \gamma = -\frac{\ddot{\eta}(r)}{[1 + \dot{\eta}^2(r)]^{\frac{3}{2}}} - \frac{\dot{\eta}(r)}{r[1 + \dot{\eta}^2(r)]^{\frac{1}{2}}}. \tag{3.8}$$

Here $\partial/\partial s$ denotes the tangential derivative along the curve $z = \eta(r)$.

For a given value of γ, the relations (2.1), (2.6), (2.7), (3.6) and (3.8) define a system of integrodifferential equations for the unknowns ρ_M, $\eta(r)$ and $\phi[r, \eta(r)]$.

4. Numerical procedure

To solve the problem (2.1), (2.6), (2.7), (3.6) and (3.8) we find it convenient to introduce the new independent variable t instead of r by the definition

$$r = \rho_M(1 - t^2). \tag{4.1}$$

This particular change of variable is chosen because near $r = \rho_M$, $\eta'(r)$ is singular. The derivative $\beta_t(t)$ of the new function $\beta(t) = \eta[r(t)]/\rho_M$ is regular at $t = 0$, which corresponds to $r = \rho_M$. Therefore we rewrite (2.1), (2.6), (2.7), (3.6) and (3.8) in terms of t, $\beta(t)$ and $\xi(t) = \phi[r(t), \rho_M \beta(t)]/\rho_M$.

Next we introduce the N mesh points t_I defined by

$$t_I = \frac{I-1}{N-1}, \quad I = 1, \ldots, N. \tag{4.2}$$

We also define the corresponding quantities

$$\beta_I = \beta(t_I), \quad I = 1, \ldots, N, \tag{4.3}$$

$$\xi_I = \xi(t_I), \quad I = 1, \ldots, N. \tag{4.4}$$

It follows from (2.1) and (2.6) that $\xi_1 = \beta_1 = 0$, so only the $N-1$ last β_I and the $N-1$ last ξ_I are unknown. We shall satisfy the equations (3.6) and (3.8) at the $N-2$ mesh points t_I, $I = 2, \ldots, N-1$. The functions $g^{\pm}$ defined in (3.7) introduce logarithmic singularities into the integrand of (3.6). We integrate these singularities by using a method similar to that of Longuet-Higgins & Cokelet (1976). The remaining part of the numerical procedure follows the work of Vanden-Broeck & Keller (1980). Details can be found in Miksis (1981).

We obtain after discretization $2N-4$ nonlinear algebraic equations for the $2N-1$ unknowns ξ_I, β_I and ρ_M. By using a three-point Lagrange extrapolation formula, we obtain two extra equations from (2.6) and (2.7). Finally we require that the curvature be equal to $\rho_M \gamma$ at $t = 1$. Thus we obtain $2N-1$ equations. This system is solved by Newton's method.

All finite-difference formulae used were accurate to at least second order, and the trapezoidal rule was used in the discretization of the integrals. For $\gamma > 0$ results of better than graphical accuracy were obtained with $N = 20$. For $\gamma < 0$ larger values of N were necessary. Convergence was checked by comparing results obtained for several values of N. Second-order Richardson extrapolation to $N = \infty$ was used when necessary. For example, for $\rho_M = 1{\cdot}4$, which is near the case of contact, we used $N = 15$, 20 and 25 and obtained $\rho_m/\rho_M = 0{\cdot}1241$, $0{\cdot}1100$ and $0{\cdot}1032$ respectively. Second-order extrapolation from the first two values to $N = 25$ yielded $0{\cdot}1037$, indicating that the results were indeed very nearly second-order accurate.

5. Results

By applying the numerical procedure described in § 4 we can find bubbles for different values of γ. Figures 1 and 2 give some examples of them. We note that for γ large (figure 1) the shape is nearly spherical. This is no surprise since as $\gamma \to \infty$ (2.4) shows that $K \sim \gamma$. Thus the bubble tends to a sphere of radius $2\gamma^{-1}$. As γ decreases the bubble becomes nearly an oblate ellipsoid with its semi-minor axis ρ_m in the direction of the flow. This nearly ellipsoidal shape was the basis of the approximate treatments of Moore (1959, 1963, 1965) and El Sawi (1974).

In figure 3 we plot the semi-major and semi-minor axes ρ_M and ρ_m versus γ. We see that ρ_M increases as γ decreases, indicating that the bubble is elongating in the direction perpendicular to the flow. The value of ρ_m initially increases until $\gamma \approx 1{\cdot}1$, after which it starts to decrease and eventually equals zero at the critical value $\gamma_0 = -0{\cdot}31$. This value of γ_0 agrees roughly with the value $-0{\cdot}26$ found in the slender-body analysis of Vanden-Broeck & Keller (1980). The smallest value of γ for which a

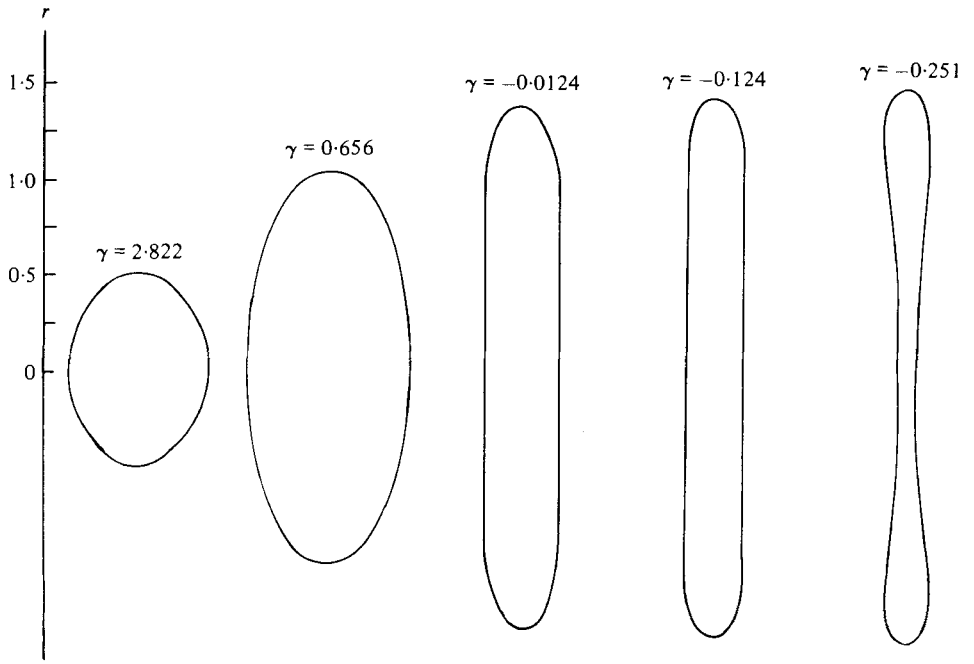

FIGURE 2. Computed bubble cross-sections for the following five values of γ (reading from left to right): 2·822, 0·656, −0·0124, −0·124, −0·251. For the first two values of γ the cross-section is nearly elliptical, while for the last value the opposite sides nearly touch. The unit of length is $2\sigma/\rho U^2$.

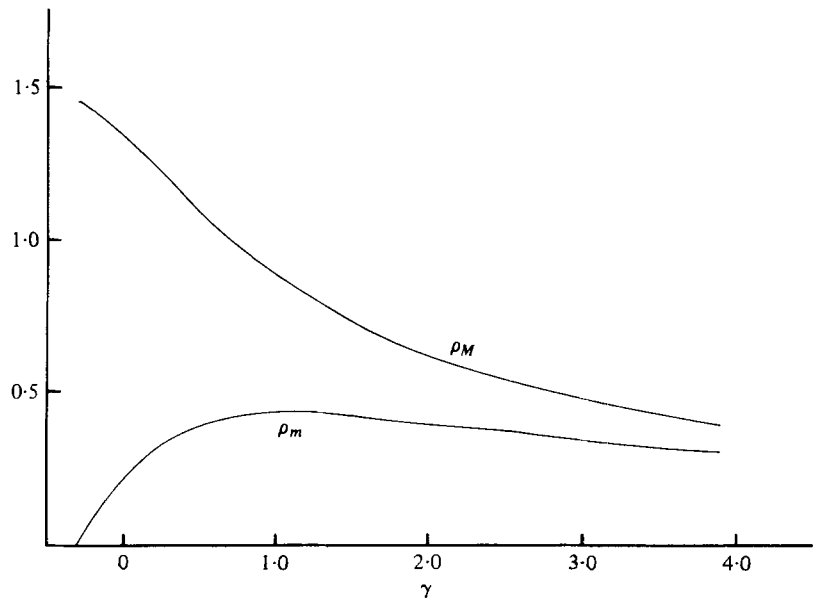

FIGURE 3. Computed values of the semi-major axis ρ_M and the semi-minor axis ρ_m of the bubble as functions of γ. The unit of length is $2\sigma/\rho U^2$. For γ large, $\rho_M \sim \rho_m \sim 2\gamma^{-1}$. At the critical value, $\gamma_0 \approx -0{\cdot}3$, opposite sides touch and $\rho_m = 0$.

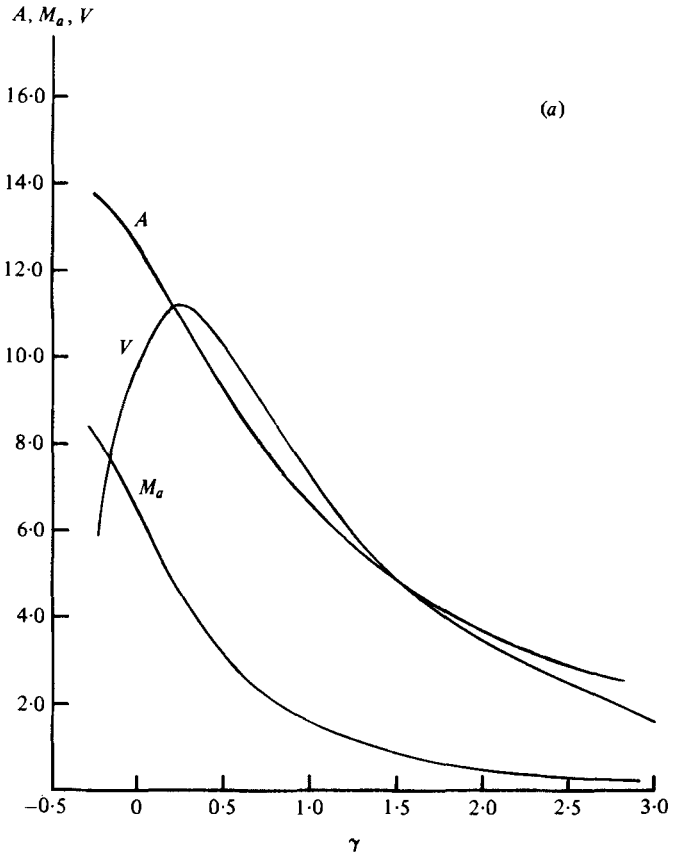

FIGURE 4 (*a*). For legend see next page.

bubble shape is shown in figure 2 is $\gamma = -0{\cdot}251$. Although this is not the critical value of γ, the bubble profile does show how the negative curvature at the stagnation point affects the bubble shape. We did not calculate the shape for smaller values of γ because the computing time would have been long.

The critical value of γ was found by extrapolation to $\rho_m = 0$ of the curve of ρ_m versus γ. The variation with γ of the bubble profile is similar to the two-dimensional case treated by Vanden-Broeck & Keller (1980).

We note from (2.4) that γ equals the curvature at the stagnation point $r = 0$. For $\gamma > 0$ the curvature at $r = 0$ is positive and the bubble is nearly an oblate spheroid. For $\gamma < 0$ the curvature is negative and the bubble profile is pinched in like an hour-glass or figure eight.

Another important parameter of the bubble is the Weber number

$$W = 2r_e \rho U^2/\sigma. \tag{5.1}$$

Here $r_e = (3V/4\pi)^{\frac{1}{3}}$ is the radius of a sphere with the same volume V as the bubble. We shall plot the properties of the bubble as functions of W as well as of γ.

In addition to the bubble shape, we have calculated its surface area A and volume V. We have also calculated the kinetic energy of the fluid when the bubble moves with

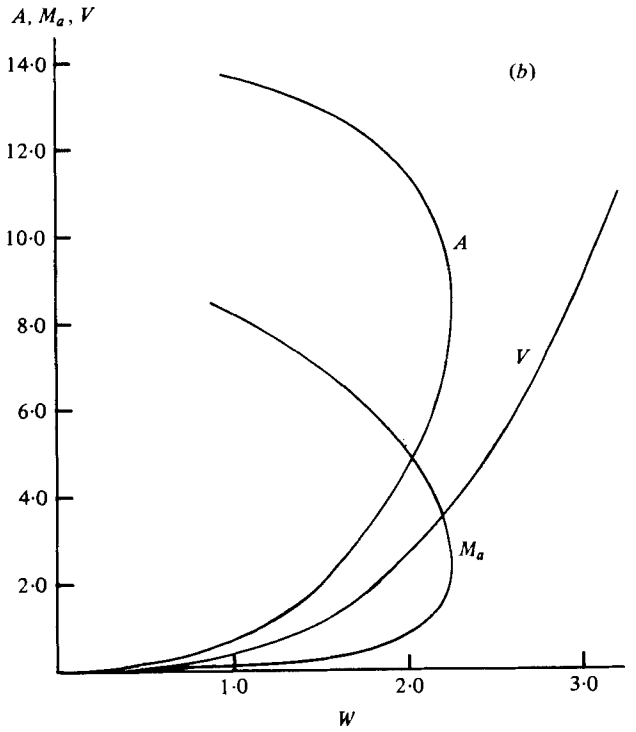

FIGURE 4. Computed values of the bubble surface area A in units of $(2\sigma/\rho U^2)^2$, the bubble volume V in units of $(2\sigma/\rho U^2)^3/5$, and the added mass M_a in units of $\rho(2\sigma/\rho U^2)^3$, (a) as functions of γ and (b) as functions of the Weber number W.

velocity U and the fluid is at rest at infinity. We write it as $\frac{1}{2}M_a U^2$, where M_a is the added mass of the bubble. These quantities are given by

$$(2\sigma/\rho U^2)^{-2} A = 4\pi \int_0^{\rho_M} r[1+\dot{\eta}^2(r)]^{\frac{1}{2}}\, dr, \tag{5.2}$$

$$(2\sigma/\rho U^2)^{-3} V = \tfrac{4}{3}\pi \left(\frac{W}{4}\right)^3 = 4\pi \int_0^{\rho_M} r\eta(r)\, dr, \tag{5.3}$$

$$(2\rho)^{-1}(2\sigma/\rho U^2)^{-3} M_a = 2\pi \int_0^{\rho_M} [\phi(r) - \eta(r)]\, r\, dr. \tag{5.4}$$

To get (5.4) we used equations in Batchelor (1967, § 6.4). In figures 4(a, b), A, V and M_a are shown as functions of γ and of W. They all tend to zero as $\gamma \to \infty$. This is because $\rho_M \to 0$ as $\gamma \to \infty$ and the bubble tends to a point. As $\gamma \to \gamma_0$ all three quantities approach non-zero finite limiting values.

Moore (1965) conjectured that there is a maximum Weber number above which the solution fails to exist. Figure 5 confirms this speculation. It is a plot of the Weber number versus the axis ratio, ρ_M/ρ_m. The maximum Weber number is $W_{\max} \approx 3{\cdot}23$ and occurs for $\rho_M/\rho_m \approx 3{\cdot}85$. Plotted along with our numerical results are those given by the approximate theories of Moore and El Sawi. We note that, after reaching a maximum, the Weber number starts decreasing and asymptotically approaches the limiting value $W \approx 2{\cdot}3$. This limit is found by using in (5.1) and (5.3) the value of V extrapolated to $\gamma = \gamma_0$.

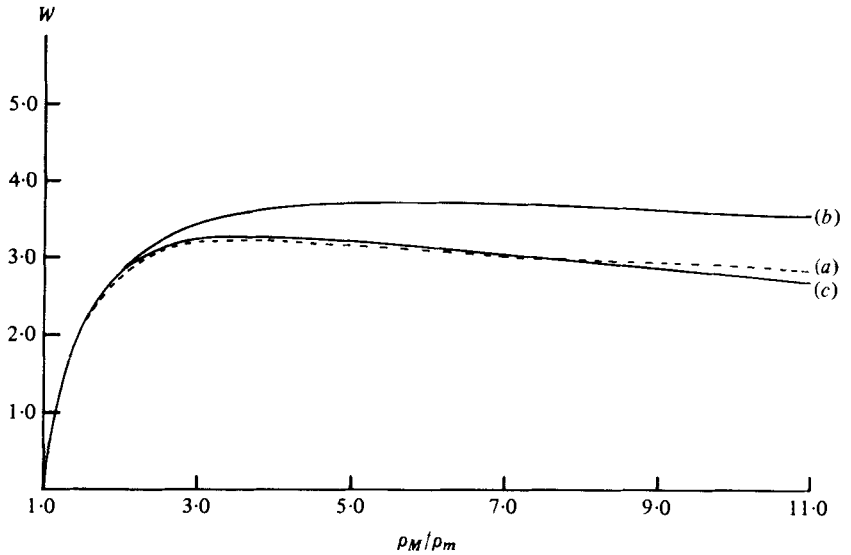

FIGURE 5. The Weber number W as a function of the axis ratio ρ_M/ρ_m as given by the present calculation (curve *a*), the two-point approximation of Moore (curve *b*), and the virial approximation of El Sawi (curve *c*). The present calculation yields $W_{\max} = 3{\cdot}23$ at $\rho_M/\rho_m \approx 3{\cdot}85$.

6. Drag and terminal velocity

When a viscous fluid flows past a bubble at a high Reynolds number, the flow is asymptotically equal to the potential flow past the bubble, except within a very thin boundary layer. Levich (1949) has shown that, for a gas bubble, the energy dissipation rate D of the flow can be found asymptotically by using this potential flow in the dissipation integral for D. Then the dissipation integral can be transformed to an integral over the surface S of the bubble to yield (see Lamb 1932, p. 581)

$$D \sim \frac{2\sigma\mu}{\rho}\int_S \frac{\partial q^2}{\partial n}ds. \tag{6.1}$$

Here μ is the viscosity coefficient and q is the dimensionless irrotational velocity of the fluid. By using (2.5) in (6.1) we find, after some calculation (see Miksis 1981), that D can be rewritten as

$$D \sim \frac{16\pi\sigma\mu}{\rho}I, \tag{6.2}$$

where the integral I is defined by

$$I = -\int_0^{\rho_M} \ddot{\eta}q^2 r(1+\dot{\eta}^2)^{-1}dr. \tag{6.3}$$

A similar formula was derived by Harper (1970, 1971).

The dissipation rate D is also equal to the power UF delivered by the force F which maintains the motion of the bubble:

$$D = UF. \tag{6.4}$$

In terms of F and the bubble density $\beta\rho$ we define the drag coefficient C_D by

$$C_D = 2F/(1-\beta)\rho U^2\pi r_e^2. \tag{6.5}$$

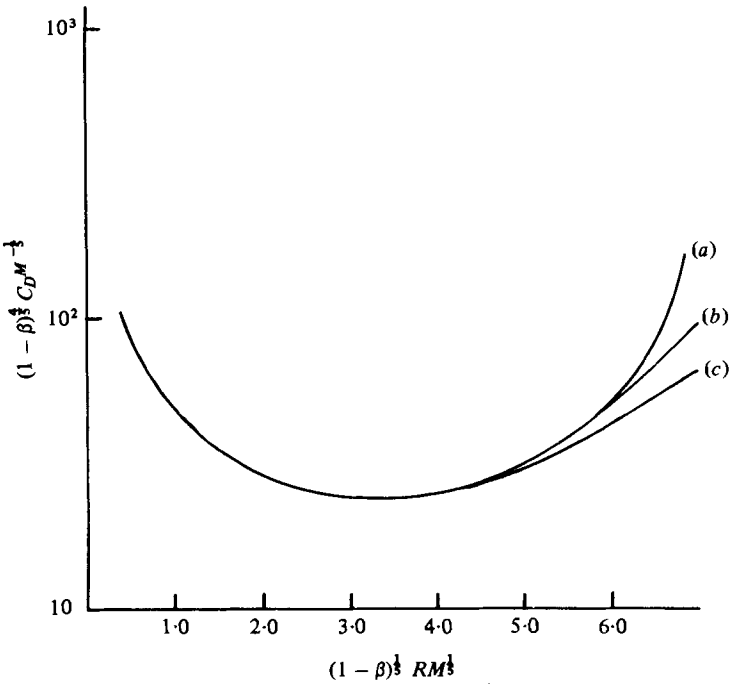

FIGURE 6. The product $C_D M^{-\frac{1}{6}}$ as a function of $RM^{\frac{1}{6}}$. Here C_D is the drag coefficient of the bubble, R is the Reynolds number based on the equivalent radius, and $M = g\mu^4/\rho\sigma^3$ is a dimensionless parameter depending only upon the fluid and gravity. Curve (*a*) is based on the present calculation, curve (*b*) on Moore's two-point approximation and curve (*c*) on El Sawi's virial approximation.

Then equations (6.2)–(6.5) lead to

$$C_D \sim \frac{32\sigma\mu}{(1-\beta)\rho^2 U^3 r_e^2} I. \tag{6.6}$$

Usually the force F on a bubble is the buoyancy force due to gravity. Upon using this force for F in (6.5) we obtain an equation for the bubble's terminal velocity U:

$$U^2 = \frac{8gr_e}{3C_D}. \tag{6.7}$$

Here g is the acceleration of gravity.

The preceding formulae can be rewritten in terms of the Reynolds number R and the dimensionless number M, which is determined mainly by the fluid. They are defined by

$$R = 2r_e \rho U/\mu, \quad M = g\mu^4/\rho\sigma^3. \tag{6.8), (6.9}$$

The Weber number W, given by (5.1), is expressible as

$$W = (4MR^4/3C_D)^{\frac{1}{3}}. \tag{6.10}$$

Now (6.6) and (6.8) can be written as

$$(1-\beta)^{\frac{1}{3}} M^{-\frac{1}{6}} C_D = 64(I^4 W^{-7}/3)^{\frac{1}{6}}, \tag{6.11}$$

$$(1-\beta)^{\frac{1}{6}} M^{\frac{1}{6}} R = 2(3IW^2)^{\frac{1}{6}}. \tag{6.12}$$

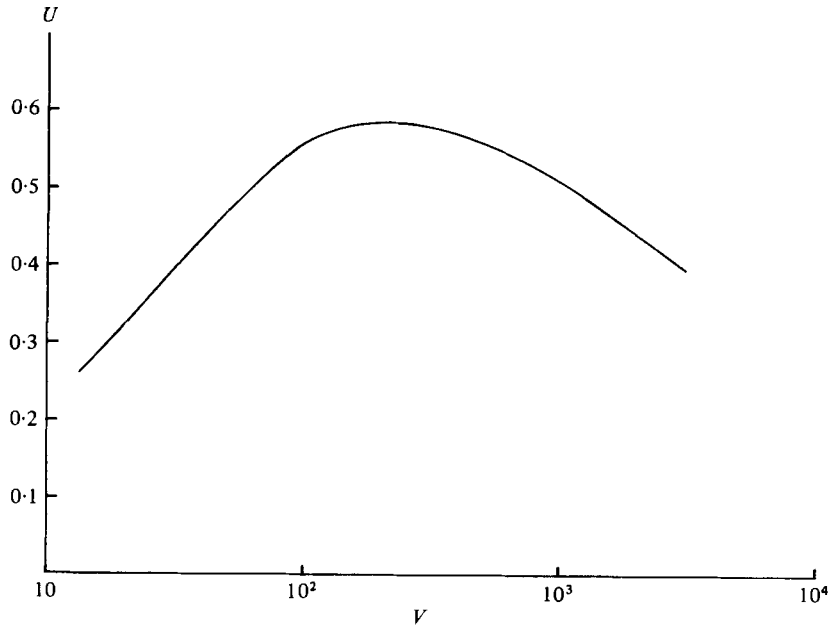

FIGURE 7. Computed values of the terminal velocity U as a function of the bubble volume V. The unit of U is $(\rho/g\mu)^{-\frac{1}{3}} M^{\frac{2}{15}}(1-\beta)^{\frac{1}{5}}$ and the unit of V is $g^{-1}\rho^{-2}M^{-\frac{1}{5}}\mu^2(1-\beta)^{-\frac{6}{5}}$.

We have used (6.11) and (6.12) to plot $M^{-\frac{1}{5}}C_D$ versus $M^{\frac{1}{5}}R$. To do so we chose γ, determined the bubble profile $\eta(r)$, calculated W from (5.3) and I from (6.3), and used these values of W and I in (6.11) and (6.12). By varying γ, we obtained the curve shown in figure 6. The minimum value of $M^{-\frac{1}{5}}C_D$ is 23·93 and it occurs at $M^{\frac{1}{5}}R = 3{\cdot}16$.

Figure 6 also shows the results of Moore (1965) and El Sawi (1974). Their approximations are in good agreement with our result for low values of $M^{\frac{1}{5}}R$, corresponding to large values of γ. Both approximate theories and our calculations show that $C_D M^{-\frac{1}{5}}$ reaches a minimum and then increases monotonically with increasing $M^{\frac{1}{5}}R$.

From (6.7), (6.8), (6.11) and (6.12) we also obtain

$$U(\rho/g\mu)^{\frac{1}{3}} M^{\frac{2}{15}}(1-\beta)^{-\frac{1}{5}} = \tfrac{1}{2}(W^3/3I)^{\frac{1}{5}}, \tag{6.13}$$

$$V(g\rho^2 M^{\frac{1}{5}}\mu^{-2})\,(1-\beta)^{\frac{6}{5}} = 32\pi(3I^6/W^3)^{\frac{1}{5}}. \tag{6.14}$$

By using (6.13) and (6.14) we have plotted the terminal velocity U versus the bubble volume V in figure 7.

This work was supported by the Office of Naval Research, the Army Research Office, the Air Force Office of Scientific Research and the National Science Foundation.

REFERENCES

BATCHELOR, G. K. 1967 *Introduction to Fluid Dynamics.* Cambridge University Press.

EL SAWI, M. 1974 *J. Fluid Mech.* **62**, 163–183.

GARABEDIAN, P. R. 1964 *Partial Differential Equations.* Wiley.

HARPER, J. F. 1970 *Chem. Engng Sci.* **25**, 342–343.

HARPER, J. F. 1971 *Chem. Engng Sci.* **26**, 501.

HARPER, J. F. 1972 *Adv. Appl. Mech.* **12**, 59–129.

HARPER, J. F. & MOORE, D. W. 1968 *J. Fluid Mech.* **32**, 367–391.

LAMB, H 1932 *Hydrodynamics.* Cambridge University Press.

LEVICH, V. G. 1949 *Zhn. Eksp. Teor. Fiz.* **19**, 18–24.

LONGUET-HIGGINS, M. S. & COKELET, E. D. 1976 *Proc. Roy. Soc.* A **350**, 1–26.

MIKSIS, M. 1981 Numerical solution of hydrodynamic free boundary problems. Ph.D. thesis, Courant Institute, New York University.

MOORE, D. W. 1959 *J. Fluid Mech.* **6**, 113–130.

MOORE, D. W. 1963 *J. Fluid Mech.* **16**, 161–176.

MOORE, D. W. 1965 *J. Fluid Mech.* **23**, 749–766.

VANDEN-BROECK, J.-M. & KELLER, J. B. 1980 *J. Fluid Mech.* **98**, 161–169.